Dendritic Transformations on Random Synaptic Inputs as Measured from a Neuron's Spike Train—Modeling and Simulation

ANDRÉ FABIO KOHN

Abstract—**Extracellular spike trains recorded from central nervous system neurons reflect the random activations from a multitude of presynaptic cells making contacts mainly on the extensive dendritic trees. The dendritic potential variations are propagated towards the trigger zone where action potentials are generated. In this paper, two dendritic propagation modes are modeled: passive and quasi-active. Synaptic bombardments are modeled as being applied apically, somatically, or distributed over the dendritic tree. The resulting simulated neuronal spike trains are analyzed by point process techniques. Dendritic inputs resulted in a tendency for random bursting, interspike interval histograms with a long tail and coefficients of variation larger than one. The autocorrelation histograms reflected dynamics of the dendritic tree and they were able to discriminate between a passive or a quasi-active propagation mode and between dendritic and somatic synaptic inputs.**

I. Introduction

NEURONS in central nervous systems are known to receive a very large number of synaptic contacts [6], [9], most of them occurring on the neurons' extensive dendritic trees, including the apical regions [33]. A noise-like membrane potential is recorded from the soma [11] in response to the ongoing presynaptic activations. This noise-like soma membrane potential is a result of the electrical filtering effect of the dendritic tree and, therefore, synaptic inputs concentrated at different parts of the dendritic tree will cause different noise processes. These, in turn, will cause statistically different spike trains to be discharged by the trigger zone. These spike trains are often the only data available for the neuroscientist because in many electrophysiological experiments dealing with central nervous systems it is only feasible to record extracellularly. This is even more true with today's emphasis on simultaneous multiunit recordings with multichannel microelectrodes [12], [13]. Therefore the techniques of spike train analysis [18], [25], [26] (this is a very partial list) are fundamental for providing information about the connectivities and dynamics of neuronal assemblies. Besides the widespread use of point-process analysis as a tool for suggesting neural pathways or showing hidden periodicities in a train of action potentials, another (less frequent) use has been in system identification [3], [5]. These identification techniques rely on cross-intensity or cross-correlation measures and, therefore, they assume the availability of *both* the inputs and the output of a specific neuron. However, as the inputs are not always experimentally available, it is important to have techniques based only on the *output* spike train to provide inferences on the neuron's functional microanatomy and physiology. Functional microanatomical inferences might include information about the region of the dendritic tree where most of the activated synapses make contacts during a certain behavior or internal state of the animal being investigated. These inferences may be of much help as it is very difficult to obtain sufficient amount of data about the microcircuitry of neuronal assemblies using fine anatomical methods, e.g., using a combination of horseradish peroxidase and electron-microscopy [34]. From a physiological standpoint, the inferences could include, for example, information about the type of dendritic transformations occurring on the multiple synaptic inputs and/or about the type of encoding carried out by the trigger zone. This task of inference from the output spike train recorded from a neuron is obviously not easy as it must necessarily rely on neuronal models. A large amount of literature has dealt with a few statistical descriptors of spike trains generated by different neuronal models, usually of the fixed threshold type, subjected to white-noise or Poisson-process inputs. These inputs have been used to mimic the random synaptic bombardment received by a neuron without considering the filtering effects of the dendritic tree (a representative list of references may be found in [20]). Tuckwell and Walsh [38] approached the mathematically difficult problem of solving the stochastic passive cable equation subjected to a two-parameter (space and time) Poisson process. The problem of first-passage time through a boundary, leading to an interspike interval, was not amenable to exact analytical solution and therefore different numerical methods were proposed to solve the equations. A single interspike interval histogram (obtained by simulation) was shown. Tuckwell *et al.* [39] using different simulation methods showed values of mean intervals, coefficients of variation, and histograms of first passage times to a fixed threshold of the membrane po-

Manuscript received January 20, 1988; revised July 20, 1988. This work was supported in part by FAPESP and SID Informática. Parts of the methodological Sections II and III were presented at the 10th Brazilian Conference on Biomedical Engineering, September 1987.

The author is with the Departamento de Engenharia de Eletricidade, Escola Politécnica, Universidade de São Paulo, São Paulo, Brasil CEP 05508.

IEEE Log Number 8824416.

tential at one end of a passive cable subjected to white-noise input applied at different distances.

In the present paper, the transformations caused by a passive or quasi-active dendritic tree on the synaptic bombardments occurring either apically or distributed all over are compared with the results obtained for synaptic bombardment directly on the soma. The effects of the synaptic inputs are measured on the spike train elicited by the target cell. A lumped parameter model is employed by approximating the dendritic system by convenient linear filters and by approximating the trigger zone by an *RC* model with an exponential threshold function. Several point-process statistics are used to analyze the trigger zone spike train. The results and concepts emerging from this work should be of help to both experimental and theoretical neuroscientists trying to gain more knowledge about the nervous system at the cellular or cellular ensemble levels.

II. The Mathematical Model and its Assumptions

A. Basic Framework

The model neuron is divided into two compartments: 1) the dendritic tree and the cell body or soma, 2) the trigger zone on the proximal region of the axon near the soma. As the modeling effort is oriented towards central neurons receiving a very large number (many thousands) of synapses, the postsynaptic potential due to a single synapse is small. The resulting local membrane potential due to a large number of randomly activated synapses is approximated by a white Gaussian continuous time random process. Experimental results seem to confirm the Gaussian hypothesis [11]. This membrane noise with a flat power spectral density is a first approximation to the resulting local haphazardly occurring membrane depolarizations and hyperpolarizations due to synaptic actions and has been used in many stochastic neuronal models [20, and references therein]. Thereafter, the postsynaptic potentials from the multiple synaptic inputs are filtered by a dendritic/somatic transfer function model. As a first approximation, it is assumed that the individual (small) postsynaptic potentials summate spatially and temporally in a linear fashion. The output from this filter is the input current to the trigger zone. The latter is modeled by a parallel *RC* circuit whose output voltage controls the genesis of action potentials. When the output voltage, from now on called the membrane potential, reaches a threshold value V_{th} the capacitor is instantaneously discharged, thereby resetting the membrane potential. An action potential firing is associated with every membrane potential resetting. The threshold can be chosen either as a constant or an exponentially varying function. In the latter case an absolute refractory period AR is followed by the threshold function $V_{\text{th}} = \theta_L + (\theta_M - \theta_L) \exp [-(t - \text{AR})/\tau_c]$ where θ_L is the steady-state threshold value, θ_M is the peak threshold value following the absolute refractory period, and τ_c is the threshold decay time constant. The dynamic description up to the time of a threshold crossing is given by the stochastic differential equation

$$C\,dx(t) + (R)^{-1}x(t)\,dt = i(t)\,dt \qquad (1)$$
$$x(t_o) = x_o, \qquad x(t) < V_{\text{th}}$$

where $x(t)$ is the membrane potential, $(R)^{-1}$ is the membrane conductance, C is the membrane capacitance, $i(t)$ is the output current from the dendritic/somatic model, x_o is the resetting or initial membrane potential, V_{th} is the threshold potential. When the multiple synaptic inputs happen on the soma, the dendritic model is bypassed (as a first approximation, the input impedance of the dendritic tree will be neglected) and, therefore, $i(t)$ is modeled as a white Gaussian noise and formally $i(t)\,dt$ in (1) should be written as $dW(t)$ where $W(t)$ is a Wiener process. This type of model is sometimes called the "leaky integrator" model and has been used in many theoretical works in neurobiology (e.g., [14], [31]). The inclusion of an absolute refractory period and an exponentially decaying-relative refractory period render the trigger zone model more similar to biological reality than the constant threshold assumption. The models used in the present work are first approximations to reality and, hence, the results obtained should be interpreted from a qualitative standpoint.

From the foregoing description, it follows that the neuron model has a continuous time/continuous state space-random input while its output is a continuous time point process. The neuron's input random process is white noise and if applied on the dendritic tree (away from the soma) it will have its power spectral density shaped by the dendritic/somatic transfer function $H(s)$ before reaching the trigger zone. The next section will describe the types of dendritic transfer functions employed in the simulations.

B. The Dendritic/Somatic Models

The first two models described below, called passive and quasi-active, represent the effects of synaptic inputs localized on dendritic shafts at a certain electrotonic region from the trigger zone. The third model, called distributed, represents a distributed injection of synaptic currents along the entire dendritic tree.

1) Passive Model: This first model describes the passive propagation of postsynaptic potentials along the dendrites and soma. The simplifying assumption is that the dendrite/soma dynamics may be approximated by that of a single cable [28] with individual postsynaptic potentials summating linearly. The starting equation is the standard cable partial differential equation. By using convenient boundary conditions [23], the transfer function relating the output current from the cable with the synaptic input current applied at the cable's origin is

$$H(s) = \text{sech}\left[\sqrt{1 + s\tau}\,\frac{l}{\lambda}\right] = \text{sech}\,[\sqrt{1 + s\tau}\,\alpha L_n] \qquad (2)$$

where τ is the membrane time constant, λ is the space constant, l is the cable length, L_n is the electrotonic length, and α is the normalized position along the cable, taking values between 0 (basal) and 1 (apical).

The amplitude response function corresponding to (2) for several physiologically meaningful parameter values shows a low-pass characteristic with a practically flat passband and a high-frequency decay with an increasing slope. For a frequency range from 0 up to about 5 times the -3 dB cutoff frequency, this frequency response function may be reasonably well approximated by a first-order transfer function. In this way, the output from this passive dendritic/somatic filter having as input a white Gaussian random process is the well-known Ornstein–Uhlenbeck random process. As a biological example, it is shown in [11] that the noise process recorded at the soma of cat motoneurons due to synaptic bombardment is Gaussian with an exponential autocorrelation function.

2) Quasi-Active Model: This second model represents the case when the dendritic/somatic membranes are in a quasi-active state [16]. The old view of the dendrites and soma was that they were always passive [35]. Today it is known that, in some types of neurons, dendrites and soma may have a nonpassive role in information propagation, having either a quasi-active or even active behavior. The quasi-active model used here is derived from the work of Koch [16] where a linearized approximation was obtained for the nonlinear membrane model of Hodgkin and Huxley. The resulting transfer impedance amplitude as a function of frequency is given in his Fig. 6 and the corresponding Laplace inverse transform is plotted in his Fig. 7. By terminating the cable with a low impedance due to the loading from the soma and/or axon, Koch's [16] figures were used as an approximate estimate of the cable's transfer function (current at end/current at origin). As there were no mathematical expressions given in his paper, $H(s)$ was estimated by taking measurements (like asymptotes, Q factor of resonant peak, peak amplitudes, and zero crossing times of the impulse response) directly from his figures. The initial estimates of parameter values were improved upon using an interactive computer program. The resulting final transfer function is

$$H(s) = \frac{1282.11s + 247082.82}{s^2 + 453s + 205209} - \frac{1200}{s + 5000}. \quad (3)$$

3) Distributed Model: This third model, derived from the passive model mentioned before, describes the power spectral density at the cable's output due to synaptic bombardment along the whole passive dendritic tree and soma. It may be shown that for large α, i.e., for apical synapses, the cutoff frequency and the dc gain are smaller than for small α, i.e., for basal or proximal synapses. Therefore, the power spectral density at the output of the filter described by (2) may be approximated by

$$S(\omega) = \frac{q(\omega_c)}{\omega^2 + \omega_c^2} \quad (4)$$

where $q(\omega_c)$ is a monotonic function increasing faster than $(\omega_c)^2$ (so as to make the dc gain larger for synapses nearer the trigger zone). To keep the mathematics simple, the following synaptic distribution will be assumed: $p(\omega_c) = 2/q(\omega_c)\pi$ for ω_c in the (arbitrary) range Ω_1, Ω_2 and $p(\omega_c) = 0$ elsewhere. This distribution assumes an increasing number of synaptic contacts towards the distal parts of the dendritic tree as a whole. The resulting power spectrum $S_T(\omega)$ of the random process at the end of the passive cable model due to the randomly occurring postsynaptic potentials distributed according to the (spatial density) function $p(\omega_c)$ is $S_T(\omega) \simeq 1/\omega$ for $\Omega_1 << \omega << \Omega_2$.

With the simplifying assumptions given above, the resulting power spectral density approximates a $1/f$ function. This $1/f$ model derivation is similar to one used in studying semiconductor noise [8]. Tuckwell and Walsh [38] computed the power spectrum of the membrane potential at one end of a cable subjected to spatially distributed white noise. They found approximately $1/f$ asymptotes at high frequencies. The upper curve of their Fig. 6 is similar to that simulated in this paper.

III. Model Simulation

The continuous time models described above had to be discretized in time for the digital simulations. The stochastic differential (1) was numerically integrated by the standard fourth-order Runge–Kutta method. The system parameters were all normalized. The RC time constant was made equal to 1 ($R = 1$ and $C = 1$) while the resetting or initial voltage x_o was always chosen equal to 0. The nonnormalized trigger zone time constant was taken as 10 ms which is a typical value for some types of cortical cells [22], [36]. When a constant threshold was desired, its value was chosen equal to 1. For the variable threshold simulations, it was assumed that the neuron had an absolute refractory period of 1.4 ms (corresponding to a normalized value 0.14), a peak threshold of 2, a steady state threshold of 1, and a time constant 3.34 ms (corresponding to a normalized value of 0.334). All other parameters from the dendritic/somatic models were normalized accordingly. With the above choice of normalizing factors, the numerical integration step size was always used equal to 0.05.

The discrete time Gaussian white sequence was generated from a uniform $U(0, 1)$ number generator using the Box–Muller [4] technique with the special care of dividing the variance by the integration step size. This was done to assure that, independently of the step size, the discrete time white sequence represented correctly the effects of the continuous time white noise.

As the objective was to compare the effects of different trigger zone input noise currents (due to different synaptic locations and different dendritic tree propagation modes) on the model neuron spike train some standardization had to be chosen. Therefore, all simulation results shown in this paper (except for one case indicated in the text) were run with a trigger zone input current variance equal to 0.323. However, the results were qualitatively independent of the input variance value. One experimental argument in favor of using the same variance for apical dendritic or somatic inputs is that, in cat motoneurons, EPSP's recorded at the soma and originating from distal

dendritic regions have similar sizes as when originating from proximal synapses [15]. Additionally, a not uncommon anatomical finding is that a single presynaptic axon may make several synaptic contacts on a dendrite [34], and when the contacts are on different dendritic branches the contacts occur at approximately the same level of the dendritic tree [7]. Different constant (dc) levels were used for the incoming noise current. Practically all of the simulation results shown in this paper refer to an input dc current equal to 1.2 (the only exception being Figs. 1(c) and 2(c) which are for dc = 0.8) although qualitatively similar results were found for the two other values employed: 0.8 and 0.5. These dc values less than 1.0 corresponded to a silent cell if no other input signal was applied. The simulations with dc = 1.2 corresponded to a cell firing spontaneously with an interspike interval of 1.792 if the threshold was a constant equal to 1, or, 1.850 if the threshold was exponentially variable with the values given above. These dc levels may be interpreted as resulting from an average of the synaptic barrage and/or from internal mechanisms of the postsynaptic cell itself.

The derivation of the discrete time versions of each of the three dendritic/somatic models required different approaches, as described in what follows.

1) Passive Model: Its output is an Ornstein–Uhlenbeck process and it may be discretized exactly using the following difference equation:

$$y(n+1) = e^{-h\omega_o} y(n) + \sqrt{(1 - e^{-2h\omega_o})\frac{\omega_o}{2}}\, u(n) \quad (5)$$

where h is the integration step size, ω_o is the -3 dB angular cutoff frequency, and $u(n)$ is a Gaussian white sequence of zero mean and variance σ^2. It is straightforward to show that the mean and autocovariance sequences of the output process from this difference equation are exact samples of the corresponding mean and autocorrelation functions from the original continuous time model. Even though the time description is exact (at the sampling times), the step-size h should be small enough to minimize aliasing. The step size used here (0.05) resulted in a -36 dB aliasing at half the sampling frequency, which was considered acceptable. Somatic or basal dendritic inputs were simulated by a white-noise current without including the loading effects of the dendritic tree. Apical dendritic inputs were supposed to be applied at an electrotonic length around 1.5, a typical value for many central nervous system neurons. A computer program was used to find the -3 dB cutoff frequency of a cable with a membrane time constant of 10 ms and the obtained value was about 150 rad/s and, hence, the normalized passive dendritic tree cutoff (angular) frequency used for the apical/passive model was 1.5.

2) Quasi-Active Model: For this model, a digital filter was designed to approximate the transfer function given by (3). The normalized resonance frequency used in the present simulations was 0.08. This resulted in a normalized cutoff angular frequency (-3 dB) equal about 2.0. Hence, the cutoff frequency is about 33 percent larger than for the passive case but with the addition of a resonant peak. For the digital filter implementation, an IIR filter was chosen due to its much faster operation. To minimize distortions in the amplitude response function, the bilinear design method was avoided. The method of choice was that of the impulse response invariance because with the integration step size used in the simulations (0.05) the resulting aliasing (the only distortion caused by this method) was very small. Equation (3) will be rewritten algebraically to make the formulas for the corresponding digital filter easier to write:

$$H(s) = a\frac{(s+b)}{(s^2 + cs + \alpha)} - \frac{\alpha}{(s+\beta)}. \quad (6)$$

The resulting digital filter using a time discretization step T is given by (7), already in a form suitable for computer implementation:

$$H(z) = a\left[\frac{\left(1 - z^{-1}q_1[q_3 + q_4 \sin(q_2)]\right)}{(1 - z^{-1}2q_1q_3 + z^{-2}q_5)}\right] - \frac{\alpha}{(1 - z^{-1}q_6)} \quad (7)$$

where

$$q_0 = \sqrt{4d - c^2}, \quad q_1 = e^{-cT/2}, \quad q_2 = q_0T/2$$
$$q_3 = \cos(q_2), \quad q_4 = (c - 2b)/q_0$$
$$q_5 = e^{-cT}, \quad q_6 = e^{-\beta T}.$$

A comment is needed on the choice of T. The continuous-time transfer function (3) has a resonant peak at about 70 Hz. The sampling interval T should be small enough to minimize the aliasing effects. On the other hand, the trigger zone model was normalized to a time constant of 1. Therefore, the relation between the 70 Hz nonnormalized resonance and the normalized resonance frequency is $0.05/T$ where 0.05 is the integration step size. For the normalized resonance peak at 0.08 the value of T is 5.714286×10^{-5}, or in other words the sampling rate is 17 500 Hz resulting in a quite acceptable aliasing error of -50 dB at a frequency equal to half the sampling rate.

3) Distributed Model: This model has at its output a power spectral density approximately of the $1/f$ type, in response to a white-noise input. Therefore, the transfer function to be approximated digitally is of the $1/\sqrt{s}$ type, which is nonrational in s. The impulse response of the latter system is proportional to $1/\sqrt{t}$. An IIR filter was chosen again instead of an FIR to maximize the simulation speed. The bilinear digital filter design method was not used due to the fact that it requires a rational transfer function in s and also because it distorts the amplitude response. The design method that appeared convenient was that of the least squares inverse design [24]. The impulse response $1/\sqrt{t}$ was sampled at every 0.0005 s, keeping the aliasing small. A computer program calcu-

lated the autocorrelation sequence of the sampled impulse response (with 1000 samples). For simplicity, a fifth-order autoregressive filter was chosen and the corresponding Toeplitz matrix was inverted using a standard computer package. The resulting digital filter was

$$H(z) = \frac{1}{\left(1 - 0.36976z^{-1} - 0.15362z^{-2} - 0.10217z^{-3} - 0.08492z^{-4} - 0.09945z^{-5}\right)}. \quad (8)$$

The amplitude response of this filter showed a reasonably good fit to the theoretical curve, the error being less than 2.5 dB in the range $[2\pi/384, 6\pi/8]$ where 2π is the normalized angular sampling frequency.

All simulation runs generated 1000 action potentials, which was found to be a reasonable compromise between statistical stability and simulation speed. Different displays of the statistical behavior of the output spike trains were used: interspike interval histogram (ISIH) and its logarithm; autocorrelation histogram (ACH), which is an estimator of the autointensity function; instantaneous rate as a function of the order (rank) of each interspike interval; scatter plot of adjacent interspike intervals; serial correlation sequence. The mean interval, the standard deviation, and the coefficient of variation (the standard deviation over the mean) were also computed for each data file, as well as the number, times of occurrence and duration of bursts within the spike train. An interval-shuffling routine was used as an aid for testing if a given spike train was renewal. The above mentioned statistics are regularly used in quantitative neurophysiological research (e.g., [25]).

Several tests were done to check the simulation and analysis programs including numerical error aspects. The results of these tests indicated that the programs were giving reliable results and therefore were adequate for the purposes of the present work.

IV. Results

The presentation of the simulation results will be divided according to the type of statistical analysis, namely: interspike interval histograms and related statistics, autocorrelation histograms, scatter diagrams, instantaneous rate, and burst detection. The results were qualitatively independent of the type threshold function (constant or exponentially variable) and input dc level employed [exemplified in Fig. 2(c)]. Therefore, practically only one set of simulations will be shown: the one with absolute refractory period followed by an exponentially decaying threshold (with the values already given above) and with an input dc = 1.2. Also, the simulations to be presented use the same 0.323 variance for the input current to the trigger zone (with a single exception). Simulations for lower intensity synaptic bombardment yielded qualitatively similar results, an exemplified in Fig. 2(c). Simulation results for random synaptic bombardment applied at half the electrotonic length of a passive dendritic tree (not shown) were qualitatively similar to the apical/passive case. For example, an exponentially decaying autocorrelation histogram resulted [similar to Fig. 2(a)], but with a correspondingly shorter time constant.

A. Interspike Interval Histogram and Related Statistics

The interspike interval histogram (ISIH) for a random presynaptic bombardment applied at apical sites of a passive dendritic tree resulted unimodal with a positive skew and with a dead time at small intervals due to the refractory period [Fig. 1(a)]. In this and all the other ISIH's, the mean interval is indicated by an arrow. The 73 longest intervals, forming a long tail in the ISIH, were not included in the graph to allow a better picture of the region around the peak. For an apical synaptic bombardment on a quasi-active dendritic tree the ISIH showed a slightly broader peak than for the passive case [Fig. 1(b)]. The histogram showed again a long tail and part of it is not shown (the 101 largest intervals were not included in the plot). Fig. 1(c) shows the ISIH for simulations of apical synaptic bombardment on a quasi-active dendritic tree with a variance equal to 10 percent of that from the previous simulations (i.e., an input variance to the trigger zone equal to 0.0323) and with an input dc = 0.8 (instead of 1.2). The histogram showed again a large peak at small intervals followed by a long tail (the ten largest intervals were not included in the plot) but this time there was a slight tendency for bimodality. When the synaptic random barrage was applied at the soma the ISIH [Fig. 1(d)] resulted with a broad peak followed by an exponential-like decay. Note that the range of the abscissa is larger than for the previous cases. The tail is quite short (the two largest intervals were not included in the plot). The ISIH for the synaptic inputs distributed along the dendritic tree [Fig. 1(e)] showed a large peak at small intervals with a long tail at large intervals (the 33 largest intervals were not plotted).

The logarithm of the ISIH's (figures not shown) indicated that for strong dendritic inputs the ISIH's [(Fig. 1(a), (b), (e)] are well described by two-exponential segments, while for somatic inputs the ISIH's are well approximated by a single exponential (except for the initial rising limb).

The mean interspike intervals (Table I) for random synaptic inputs added to an input dc = 1.2 to the trigger zone, were all smaller than the spontaneous firing period of a cell driven solely by a dc = 1.2 (i.e., without random inputs). The coefficient of variation (CV) (Table I) was larger than 1.0 for all dendritic inputs and smaller than 1.0 for somatic inputs. Even in the case of a much lower input variance (10 percent of the value used before) to a quasi-active model [corresponding to the ISIH of Fig. 1(c)] the CV was larger than one. In this last simulation, the dc was 0.8 and hence it corresponds to a spontaneously silent cell. The low level synaptic bombardment makes it fire with a mean interval 3.389.

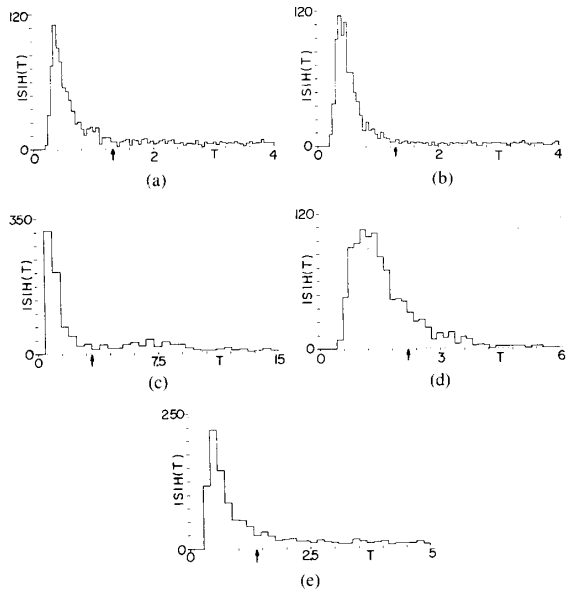

Fig. 1. Interspike interval histograms (ISIH). In this, as well as in Figs. 2 and 3, the abscissae are in arbitrary units corresponding to the normalized model parameters. The arrow at the horizontal axis indicates the mean interval. Part of the long tails have been ommitted for graphical clarity and the number of intervals not included in the histograms are indicated by #ini. (a) Apical/passive model, binwidth (bw) = 0.0506, #ini = 73. (b) Apical/quasi-active model, bw = 0.0506, #ini = 101. (c) Apical/quasi-active model with trigger zone input variance 0.0323 and dc = 0.8, bw = 0.5, #ini = 10. (d) Somatic model, bw = 0.15, #ini = 2. (e) Distributed model, bw = 0.15, #ini = 33.

TABLE I
MEAN INTERVAL AND COEFFICIENT OF VARIATION

	Apical				
	Pass.	Quas. Act.	Somatic	Distrib.	Noiseless
Mean interval	1.337	1.285	1.619	1.395	1.850
	—	3.389*	—	—	—
Coefficient of Variation	1.282	1.435	0.507	1.103	0.000
	—	1.110*	—	—	—

*for 0.0323 trigger zone input variance and dc = 0.8.

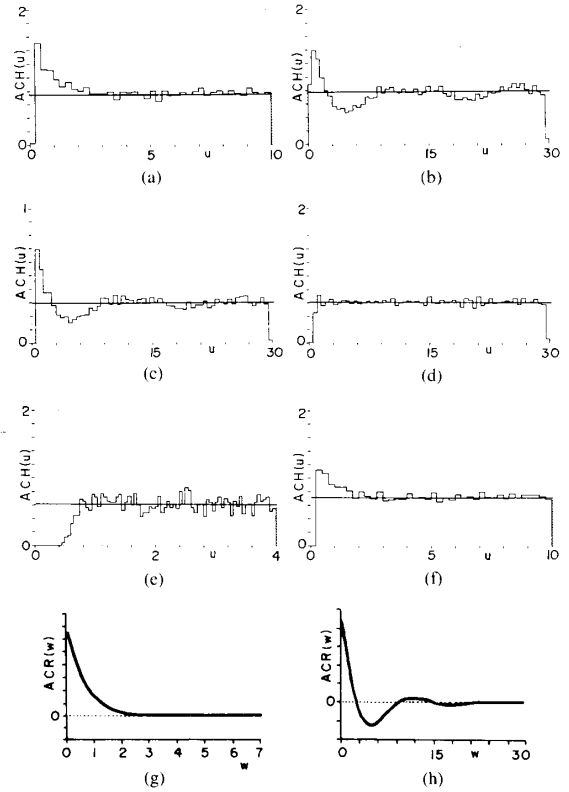

Fig. 2. Autocorrelation histograms of the spike trains (ACH) and autocorrelation functions for the dendritic output noise. The horizontal lines indicate the mean rate. (a) Apical/passive model, bw = 0.251. (b) Apical/quasi-active, bw = 0.517. (c) Apical/quasi-active model with trigger zone input variance 0.0323 and dc = 0.8, bw = 0.517. (d) Somatic, bw = 0.517. (e) Somatic, bw = 0.0506, this figure shows the details of the previous figure for small lags. (f) Distributed model, bw = 0.251. (g) Theoretical autocorrelation function of the output noise from the apical/passive dendritic tree model. (h) Theoretical autocorrelation function of the output noise from the apical/quasi-active dendritic tree model. In both (g) and (h) the ordinates are in arbitrary units. The abscissae are in the same time scales as those used in the corresponding autocorrelation histograms (a) and (b/c).

B. *Autocorrelation Histogram*

The ACH for the apical/passive case [Fig. 2(a)] showed a large peak for small lags followed by an exponential-like decay towards the mean-rate value, indicated by a horizontal line. Obviously, near zero lags the ACH is zero due to the refractory period. Note that the ACH's are calibrated in rate units (a probability estimate divided by the bin width). The ACH for the apical/quasi-active model [Fig. 2(b)] showed higher than average rates for lags up to about 2.4 and smaller than average rates for lags in the range 2.4–8.5. This is in contrast with the passive case where a monotonic decrease was found. When the same apical/quasi-active model was subjected to a much smaller input variance (10 percent of the previous value) with a trigger zone dc current equal to 0.8 the ACH [Fig. 2(c)] still showed the biphasic nature described above. When the synaptic barrage was applied somatically, the ACH resulted flat [Fig. 2(d)] except for the small lags where it was zero and then raised to the mean rate plateau value [Fig. 2(e)]. For the distributed model, the ACH showed a positive peak [Fig. 2(f)] followed by a monotonic decrease towards the mean rate value. Fig. 2(g) and (h) show the theoretical autocorrelation functions of the output current from the passive and quasi-active dendritic models (i.e., the input current to the trigger zone), respectively. They are quite remindful of Fig. 2(a) and (b), respectively. The time constants for Fig. 2(a) and (g) are practically the same, and the first two zero crossings occur at identical lags in Fig. 2(b), (c), and (h).

C. *Scatter Diagram*

The scatter diagrams are shown for adjacent intervals in the range from 0 to 5. The scatter plots corresponding

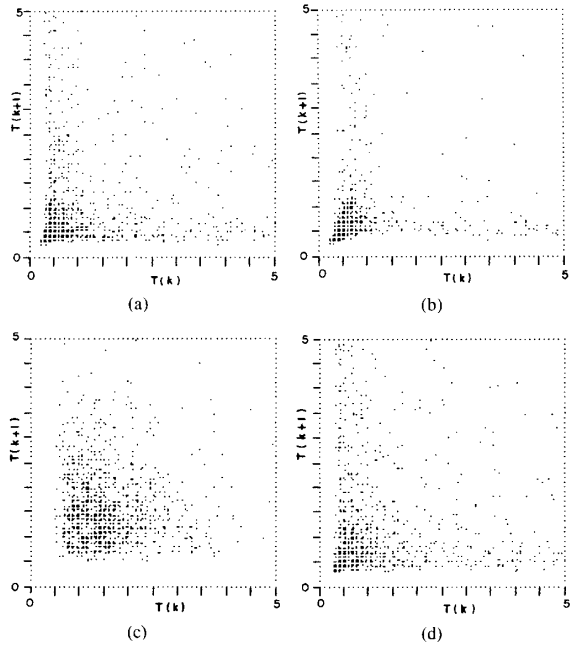

Fig. 3. Scatter diagrams. For clarity purposes all the scatter diagrams show adjacent intervals only in the range from 0 to 5. The number of points not included is indicated by #pni. (a) Apical/passive model, #pni = 82. (b) Apical/quasi-active model, #pni = 159. (c) Somatic model, #pni = 10. (d) Distributed model, #pni = 67.

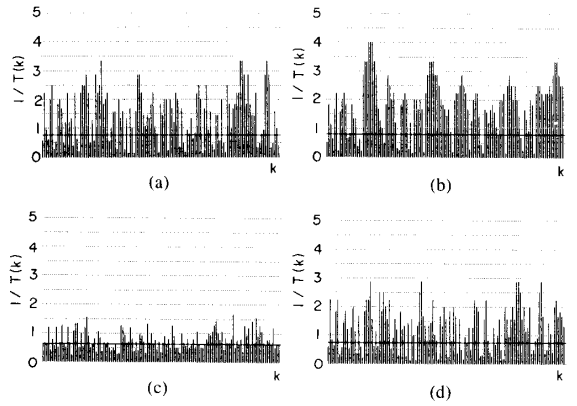

Fig. 4. Instantaneous rate as a function of the order. The first 125 intervals $T(k)$, $k = 1,125$ are plotted as $1/T(k)$ as a function of k. The horizontal lines indicate the mean rate. (a) Apical/passive model. (b) Apical/quasi-active model. (c) Somatic model. (d) Distributed model.

TABLE II
AVERAGE BURST STATISTICS

	A/P	A/Q-A	Somatic	Distrib.
# bursts/train	17	34	0	7
Average # of spikes/burst	7.00	8.82	0.00	7.29
Average intra-burst interval in % of spike train mean interval	29.0	30.6	0.00	31.2

A/P = apical passive; A/Q-A = apical quasi-active.

to simulations with dendritic inputs [Fig. 3(a), (b), (d)] indicated varying degrees of positive correlation for small intervals, the higher correlated being the apical/quasi-active case. In this case there was a strong predominance of short intervals and a paucity of medium and large intervals. Inputs to the soma were seen to cause no correlation between adjacent intervals [Fig. 3(c)]. The correlation coefficients for the plots of Fig. 3 were 0.173, 0.403, −0.018, and 0.135, respectively. The ACH of the shuffled interspike intervals showed differences from the unshuffled case in the same proportion as the correlation coefficients for Fig. 3, i.e., the largest differences were for the apical/quasi-active and there was no difference for the somatic synaptic inputs.

D. Instantaneous Rate and Burst Statistics

In Fig. 4 each plot shows the first 125 "instantaneous rates" within each simulated spike train (instantaneous rate defined as the inverse of an interspike interval). The horizontal lines indicate the respective mean rates. The profile of the figure for the apical/passive case [Fig. 4(a)] indicates the existence of short bursts occurring at random times and with random durations. For the apical/quasi-active case, the tendency for bursting was more pronounced [Fig. 4(b)] while for the somatic inputs there was no indication of bursting [Fig. 4(c)]. Finally, the profile for the distributed case showed only a slight indication of bursting [Fig. 4(d)].

A simple definition for a burst was employed in a program devised to search for bursts in a spike train. A sequence of action potentials was defined as a burst if at least M consecutive action potentials occurred with corresponding interspike intervals less than or equal to a certain value T_{max}. The results of Table II were obtained by taking $M = 6$ and T_{max} as the mean interval divided by 2.5. The number of bursts within each record of 1000 action potentials was smaller (one half) for the apical/passive than for the apical/quasi-active case. It decreased for the case of distributed synaptic inputs while the somatic synaptic barrages caused no bursting at all. The number of action potentials in a burst and the average intraburst interspike intervals (measured in percentage of the spike train mean interval) were practically independent of the type of dendritic model or synaptic barrage localization, except for the somatic inputs.

V. DISCUSSION

Central neurons show, to varying degrees, a segregation of synaptic inputs on their dendritic trees. Presynaptic fibers coming from different origins make contacts at different levels of the dendritic tree, one example being the neurons in the hippocampus [1]. The ubiquitous layered structure of cortices and the alignment of dendritic trees are well-suited for the existence of segregated inputs to dendritic trees. The specific region of synaptic activations as well as the types of dendritic propagation and

trigger zone encoding are fundamental factors that define how a neuron processes incoming information during a certain state or behavior.

All the mean intervals shown in Table I for simulations with random synaptic inputs are smaller than the interval resulting by applying only the 1.2 dc input current. This means that, for the trigger-zone model and the input intensities employed, the addition of synaptic bombardment noise results in an increase in the mean firing rate. It should be pointed out that if a white-noise input plus a dc current are applied to a pure integrator model with constant threshold, the resulting spike-train mean interval is equal to that without the noise input. But for the leaky integrator (with fixed threshold) it has been shown that the spike train mean rate increases with the input white noise variance [29]. Our simulations showed this to be true for much more general cases, i.e., nonwhite noise and time-varying threshold. An example of an experimental evidence is found in [10] where white-noise length disturbances cause discharge rate increases in a stretch receptor neuron. The current reaching the receptor cell's trigger zone has its power spectral density shaped by mechanical filtering. Another example is given later on.

The interspike interval coefficient of variation (CV) was smaller than 1 only for the somatic inputs. For all dendritic inputs, the CV was larger than 1, independent of location (apical or distributed), type of propagation, type of threshold, and input dc current value (Table I). The dependence of the CV on the input intensity was not analyzed exhaustively but it showed a clear positive correlation. A simulation for the apical/quasi-active model with a ten-times lower input power still resulted in CV $>$ 1, although smaller than for the higher variance case. These high CV's were a consequence of the long tails found in the ISIH's. This widespread finding of larger-than-one CV's for dendritic inputs seems to be a possible explanation for the experimentally found larger-than-one CV's (e.g., [19], [21]). In [19] about 45 percent of the mesencephalic reticular formation cells analyzed showed CV $>$ 1. The CV range was between 0.09 and 3.1 (with a mode near 0.9) and a possible explanation for this finding is provided by our simulations: part of the cell population might be receiving either very little synaptic input or mainly somatic drive with very little dendritic contributions while the other part is primarily being driven by dendritic inputs. In [21] white-noise modulation of an adapting light applied to single goldfish ganglion cells caused the mean CV's to increase from 0.92 (in steady illumination) to 1.57. At the same time the mean discharge rate increased from 38.5/s to 58.3/s. As there is a filtering effect in the retina [21], these results seem to be a real life equivalent of some of the simulation results presented here. The experimental fact that the coefficient of variation could result larger than 1 in actual neurons (a Poisson process has CV = 1) has puzzled some neuroscientists. Tuckwell [37] had proposed that for CV $>$ 1 there should be a substantial amount of inhibition to cause a long tail in the ISIH. Wilbur and Rinzel [42] proposed that a superexcitable phase for the neuron was a better candidate to provide CV $>$ 1. Using a model with a superexcitable phase following a refractory phase they obtained CV's of the order of 1.17. To obtain larger CV's, they used a somewhat less realistic model where there was no refractoriness but only a superexcitable phase following a spike. While a superexcitable phase is found in some peripheral axons (following a period of refractoriness) it is not clear if it is a common finding in central neurons. Certainly dendritic synaptic bombardment, as analyzed here in this paper, is a common finding in nature and therefore a probable cause for many of the experimentally described CV's larger than 1. Tuckwell *et al.* [39] obtained CV $>$ 1 for very high firing rates in a passive cable subjected to a white-noise input current applied at the vicinity of the trigger zone characterized by a constant threshold. For farther synaptic inputs the CV's were less than 1, perhaps due to small input intensities.

The ISIH's for dendritic inputs all showed quite long tails which are explainable by the fact that low-pass filtered noise tends to cause epochs of high activity and epochs of very low activity (i.e., very short and very long interspike intervals, respectively). They were all unimodal, except in Fig. 1(c) where there was a slight tendency for bimodality, and positively skewed as are the ISIH's of many cells in nature. Nevertheless, there are neurons that have quite different ISIH's [27] and therefore, more complicated dynamics than those covered in our simulations must be involved. Webb [40], [41], using visual and auditory cortical cells in the cat, studied the first-order statistics when the animal was in different states: awake, asleep (quiet and rem), and alarmed. On passing from the asleep state to the awake state, the average finding was that the mean rate, the CV, and the skewness decreased. In our simulations, those same changes in mean rate, CV, and skewness occur when the synaptic barrage is moved from a dendritic site towards or nearer the cell body. One class of cells in Webb's [41] experiments also showed a further decrease in the above mentioned parameters when the animal was alarmed by a hissing noise. The study of the mechanisms underlying the different states of alertness or levels of arousal in the cortex should be a multipronged activity, involving not only the biochemical and endocrine but also the microanatomic and electrophysiologic approaches. For the latter two, theoretical and simulation results (as found in this and other papers) should provide conceptual tools to help the experimenter in the interpretation of his results as well as in the planning of new experiments (physiological and/or anatomical).

No outstanding differences were found between a passive and a quasi-active dendritic tree with respect to mean interval, CV, and ISIH of the trigger zone spike trains. But an interesting difference appeared in the autocorrelation histogram (ACH). For the apical/passive simulation the autocorrelation was exponentially decreasing [Fig. 2(a)] while for the apical/quasi-active it showed an undershoot [Fig. 2(a) and (c), respectively]. A quite interesting observation was that the shapes of each ACH fol-

lowed approximately the autocorrelation function of the output noise from the corresponding dendritic tree (the input current noise to the trigger zone) (Fig. 2(g), (h)]. The same applied to the distributed case but is not shown. From these findings it may be proposed that after obtaining the autocorrelation histogram of a given spike train one may compute its Fourier transform to obtain an estimate of the amplitude response of the dendritic tree equivalent filter (except for a multiplying constant factor) assuming that the equivalent local synaptic input effects are white. This finding relating membrane noise statistics to spike-train statistics should be investigated experimentally and mathematically (a relevant approach is seen in [3]) so that the effects on the spike train caused by the dendritic tree and the trigger zone dynamics should be clearly evidenced. From the results above, if the ACH of a neuron's spike train changes from monotonic to biphasic, or vice versa (perhaps associated with different experimental or behavioral conditions), then the experimenter may hypothesize that there was a change in the propagation mode in the dendritic tree (clearly other hypotheses are also possible). A passive propagation causes a different probability of firing at the trigger zone conditioned on a previous firing when compared with a quasi-active propagation, as evidenced by the ACH (this effect might be looked at as an ultrashort neuronal memory). This means that two spike trains generated by these two differently functioning dendritic trees will have different firing patterns and, therefore, these spike trains will probably have different effects on their postsynaptic neurons. If a central nervous system neuron shows a monotonically decaying ACH [like in Fig. 2(a) and (f)] or a biphasic ACH [like in Fig. 2(b) and (c)] one can say that there is no rhythmic firing and that a reasonable hypothesis is that the synaptic bombardment is not restricted to the soma but has considerable dendritic sources. Many complicating factors are possible, such as strong synaptic inhibitory inputs at or near the soma. Our data and the concepts behind them are helpful in hypothesis-making but they cannot rule out other effects. The complexities of the nervous system seldom allow very strong inferences to be made from available data and, therefore, any additional conceptual results, even if not absolute, are a welcome addition to the armamentarium currently available to the neuroscientist.

In the present simulations, spike trains caused by somatic inputs showed a flat ACH and uncorrelated interspike intervals therefore indicating a very random spike train and suggesting that the point process is renewal. On the other hand, for the dendritic inputs, the scatter plots showed a positive correlation (smaller for the passive case) for small intervals, and the shuffled spike trains showed changes in their ACH (smaller for the passive case) thus suggesting that the renewal hypothesis is not acceptable. Thus, neuronal models that include simple dendritic dynamical descriptions seem sufficient to cause nonzero serial correlation (at least for small intervals) without the needed to postulate special trigger zone dynamics. It should be pointed out that quite similar results were obtained for fixed threshold simulations, although they were not shown. In nature, a variety of serial correlations and scatter plots have been found. Two examples reminding the scatter plots presented above are seen in [30]. Our Fig. 3(a), (b), and (d) are similar to the scatter plot of their unit 240-1, while our Fig. 3(c) is similar to the scatter plot of their unit 259-2.

Many of the results presented above are explainable, at least in part, by the tendency for bursting evidenced by Fig. 4(a), (b), and (d) and corroborated by Table II. Different average burst rates (number of bursts/train) were generated by the passive (17) and quasi-active (34) dendritic models. Nevertheless, it should be clear that the average burst rate is only useful for differential (i.e., relative or comparative) discrimination (e.g., during changes associated with different behavioral states). For a single spike-train record, only the autocorrelation histogram may tell the type of dendritic propagation. Bassant [2] gives statistical descriptions of the spontaneous firing of pyramidal cells of the rabbit dorsal hippocampus. He classified the cells in five groups according to their statistical characteristics. Three of the groups showed random bursting and it is interesting to note that his group E (CV = 1.55, long tailed positively skewed ISIH, peaked ACH with monotonic decay towards mean rate, scatter plot with positive correlation for small intervals) is well matched by our results for the passive model (apical or distributed). On the other hand, his group A (CV = 0.65, short positively skewed ISIH, flat ACH, scatter plot without correlations) seems well representable by our somatic synaptic input model. Still another set of experimental data that show resemblances to the simulation results is seen in [17]. They compared the spike-train statistics of neurons in the ventrolateral nucleus of the thalamus during sleep and wakefulness. They found that a broad-peak ISIH and a flat ACH in the awake state turned during sleep into a larger CV (>1), a sharp-peaked ISIH at small intervals, and an ACH with a monotonic decrease to the mean-rate plateau. Again, these parallels between experimental findings and our simulation results are not intended to point to definitive explanations but rather to suggest a plausible hypothesis about mechanisms and to evidence that the availability of these types of simulation results may enhance the yield from experimental research. So, instead of only recording and describing the data, one might try to hypothesize mechanisms behind the findings and possibly go after their experimental confirmation or rebuttal, thereby enriching the knowledge about the phenomena under study.

Different situations from those described in this paper can be simulated using a similar approach. For example, if a different synaptic distribution is postulated for a passive dendritic tree it is sufficient to find the corresponding power spectral density $S_T(\omega)$ and then design a new digital filter that will simulate the dendritic dynamics. If presynaptic random inputs are activated mainly at two different regions of a passive dendritic tree (i.e., at two

different electrotonic lengths of the equivalent cable) then, assuming linearity, two simple digital filters of the form (5) with different cutoff frequencies will be associated in parallel to produce the input current to the trigger zone.

As already mentioned before, the approach and the results of this paper are also relevant to the study of sensory receptors as the receptor potential is a filtered version of the externally-applied sensory stimulus. The filtered membrane potential is encoded by the trigger zone producing the afferent spike train. The filtering is due to the peripheral apparatus of the sensory transducer and its characteristics depend on the particular receptor. An example remindful of the apical/quasi-active dendritic model is given by eccentric cells in *Limulus* that show a generator potential power spectrum of the low-pass type with a resonant peak [32]. The autocorrelation histogram of the spike train was very similar to our Fig. 2(b) and (c) even though the histogram had a different definition (it was the autocorrelation of a continuous state-space random process obtained from the spike train by assigning a constant value, equal to the instantaneous rate, between the times of discharge of two consecutive spikes). Therefore, in sensory physiology, the autocorrelation histogram is a potentially useful indicator of sensory transduction processes.

Acknowledgment

The author would like to thank C. Itiki for her invaluable help in the computer programming.

References

[1] P. Andersen, "Operational principles of hippocampal neurons," in *Neurobiology of the Hippocampus*, W. Seifert, Ed. London: Academic, 1983.

[2] M. H. Bassant, "Analyse statistique de l'activité des cellules pyramidales de l'hippocampe dorsal du lapin," *Electroencephalogr. clin. Neurophysiol.*, vol. 40, pp. 585-603, 1976.

[3] H. van den Boogaard, G. Hesselmans, and P. Johannesma, "System identification based on point processes and correlation densities. I. The nonrefractory neuron model," *Math. Biosci.*, vol. 80, pp. 143-171, 1986.

[4] G. E. P. Box and M. E. Miller, "A note on the generation of random normal deviates," *Ann. Math. Statist.*, vol. 29, pp. 610-611, 1958.

[5] D. R. Brillinger, H. L. Bryant, and J. P. Segundo, "Identification of synaptic interactions," *Biol. Cybern.*, vol. 22, pp. 213-228, 1976.

[6] A. Brodal, *Neurological Anatomy*. New York: Oxford, 1981.

[7] A. G. Brown and R. E. W. Fyffe, "Direct observations on the contacts made between Ia afferent fibres and α-motoneurones in the cat's lumbosacral spinal cord," *J. Physiol.*, vol. 313, pp. 121-140, 1981.

[8] M. J. Buckingham, *Noise in Electronic Devices and Systems*. Chichester: Ellis Northwood, 1983.

[9] T. H. Bullock, R. Orkand, and A. Grinnell, *Introduction to Nervous Systems*. San Francisco: Freeman, 1977.

[10] W. Buno, J. Fuentes, and J. P. Segundo, "Crayfish stretch-receptor organs: Effects of length-steps with and without perturbations," *Biol. Cybern.*, vol. 31, pp. 99-110, 1978.

[11] W. H. Calvin and C. F. Stevens, "Synaptic noise and other sources of randomness in motoneuron interspike intervals," *J. Neurophysiol.*, vol. 31, pp. 574-587, 1968.

[12] H. Eichenbaum and M. Kuperstein, "Extracellular neural recording with multichannel microelectrodes," *J. Electrophysiol. Tech.*, vol. 13, pp. 189-209, 1986.

[13] G. L. Gerstein, M. J. Bloom, I. E. Espinosa, S. Evanczuk, and M. R. Turner, "Design of a laboratory for multineuron studies," *IEEE Trans. Syst., Man, Cybern.*, vol. SMC-13, pp. 668-676, 1983.

[14] A. V. Holden, *Models of the Stochastic Activity of Neurones*. Berlin: Springer, 1976.

[15] R. Iansek and S. Redman, "The amplitude, time course, and charge of unitary excitatory postsynaptic potentials evoked in spinal motoneurone dendrites," *J. Physiol.*, vol. 234, pp. 665-688, 1973.

[16] C. Koch, "Cable theory in neurons with active, linearized membranes," *Biol. Cybern.*, vol. 50, pp. 15-33, 1984.

[17] Y. Lamarre, M. Filion, and J. P. Cordeau, "Neuronal discharges of the ventrolateral nucleus of the thalamus during sleep and wakefulness in the cat—I: Spontaneous activity," *Exp. Brain Res.*, vol. 12, pp. 480-498, 1971.

[18] J. P. Landolt and M. J. Correia, "Neuromathematical concepts of point process theory," *IEEE Trans. Biomed. Eng.*, vol. BME-25, pp. 1-12, 1978.

[19] P. Lansky and T. Radil, "Statistical inference on spontaneous neuronal discharge patterns," *Biol. Cybern.*, vol. 55, pp. 299-311, 1987.

[20] P. Lansky and V. Lanska, "Diffusion approximation of the neuronal model with synaptic reversal potentials," *Biol. Cybern.*, vol. 56, pp. 19-26, 1987.

[21] M. W. Levine, "Retinal processing of intrinsic and extrinsic noise," *J. Neurophysiol.*, vol. 48, pp. 992-1010, 1982.

[22] H. D. Lux and D. A. Pollen, "Electrical constants of neurons in the motor cortex of the cat," *J. Neurophysiol.*, vol. 29, pp. 207-220, 1966.

[23] R. J. MacGregor and E. R. Lewis, *Neural Modeling*. New York: Plenum, 1977.

[24] A. V. Oppenheim and R. W. Schafer, *Digital Signal Processing*. Englewood Cliffs, NJ: Prentice-Hall, 1975.

[25] D. H. Perkel, G. L. Gerstein, and G. P. Moore, "Neuronal spike trains and stochastic point processes—I: The single spike train," *Biophys. J.*, vol. 7, pp. 391-418, 1967.

[26] ——, "Neuronal spike trains and stochastic point processes—II: Simultaneous spike trains," *Biophys. J.*, vol. 7, pp. 419-440, 1967.

[27] G. F. Poggio and L. J. Viernstein, "Time series analysis of impulse sequences of thalamic somatic sensory neurons," *J. Neurophysiol.*, vol. 27, pp. 517-545, 1964.

[28] W. Rall, 'Core conductor theory and cable properties of neurons," in *Handbook of Physiology, Vol. 1*, E. R. Kandel, Ed. Bethesda, MD: Amer. Physiol. Soc., 1977.

[29] L. M. Ricciardi and L. Sacerdote, "The Ornstein-Uhlenbeck process as a model for neuronal activity," *Biol. Cybern.*, vol. 35, pp. 1-9, 1979.

[30] R. W. Rodieck, N. Y.-S. Kiang, and G. L. Gerstein, "Some quantitative methods for the study of spontaneous activity of single neurons," *Biophys. J.*, vol. 2, pp. 351-368, 1962.

[31] J. P. Segundo, D. H. Perkel, H. Wyman, H. Hegstad, and G. P. Moore, "Input-output relations in computer-simulated nerve cells," *Kybernetik*, vol. 4, pp. 157-171, 1968.

[32] R. Shapley, "Fluctuations of the impulse rate in Limulus eccentric cells," *J. Gen. Physiol.*, vol. 57, pp. 539-556, 1971.

[33] G. M. Shepherd, *The Synaptic Organization of the Brain*. New York: Oxford Univ., 1979.

[34] P. Somogyi, Z. F. Kisvarday, K. A. C. Martin, and D. Whitteridge, "Synaptic connections of morpholocally identified and physiologically characterized large basket cells in the striate cortex of the cat," *Neuroscience*, vol. 10, pp. 261-294, 1983.

[35] W. A. Spencer, "The physiology of supraspinal neurons in mammals," in *Handbook of Physiology, Vol. 1*, E. R. Kandel, Ed. Bethesda, MD: Amer. Physiol. Soc., 1977.

[36] C. E. Stafstrom, P. C. Schwindt, and W. E. Crill, "Cable properties of layer V neurons from cat sensorimotor cortex in vitro," *J. Neurophysiol.*, vol. 52, pp. 278-289, 1984.

[37] H. C. Tuckwell, "Synaptic transmission in a model for stochastic neural activity," *J. Theoret. Biol.*, vol. 77, pp. 65-81, 1979.

[38] H. C. Tuckwell and J. B. Walsh, "Random currents through nerve membranes," *Biol. Cybern.*, vol. 49, pp. 99-110, 1983.

[39] H. C. Tuckwell, F. Y. M. Wan, and Y. S. Wong, "The interspike interval of a cable model neuron with white noise input," *Biol. Cybern.*, vol. 49, pp. 155-167, 1984.

[40] A. C. Webb, "The effects of changing levels of arousal on the spontaneous activity of cortical neurones—I: Sleep and wakefulness," *Proc. Roy. Soc. London B.*, vol. 194, pp. 225-237, 1976.

[41] A. C. Webb, "The effects of changing levels of arousal on the spontaneous activity of cortical neurones—II: Relaxation and alarm," *Proc. Roy. Soc. London B.*, vol. 194, pp. 239-251, 1976.

[42] W. J. Wilbur and J. Rinzel, "A theoretical basis for large coefficient of variation and bimodality in neuronal interspike interval distribution," *J. Theoret. Biol.*, vol. 105, pp. 345-368, 1983.

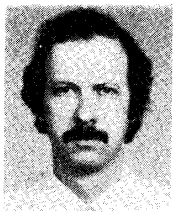

André Fabio Kohn was born in São Paulo, Brasil, in 1951. He received the B.S., and the M.S., degrees in electrical engineering from the Escola Politécnica, Universidade de São Paulo, and the Ph.D. degree in engineering from the University of California, Los Angeles, in 1973, 1976, and 1980, respectively. His doctoral research was done at UCLA's Brain Research Institute.

He currently teaches signal processing, system theory, and neural modeling at the Escola Politécnica, Universidade de São Paulo, São Paulo, Brasil. He also directs a small biomedical engineering laboratory in the same University. His research interests include theoretical and experimental neurophysiology, biological signal processing, quantitative methods in neurological electrodiagnosis. He received UCLA's Crump Award for Excellence in Medical Engineering in 1980.